Optical Materials 140 (2023) 113879

Contents lists available at ScienceDirect

Optical Materials

journal homepage: www.elsevier.com/locate/optmat

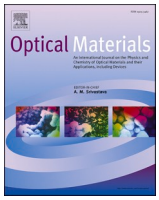

Research Article

Optical simulation and experimental investigation of the crystalline silicon/black silicon/perovskite tandem structures

Gagik Ayvazyan [a,*], Ferdinand Gasparyan [b], Vladimir Gasparian [c]

[a] National Polytechnic University of Armenia, 105, Teryan, Yerevan, 0009, Armenia
[b] Yerevan State University, 1, Alex Manoogian, Yerevan, 0025, Armenia
[c] California State University, Bakersfield, CA, USA

ARTICLE INFO

Keywords:
Perovskite
Black silicon
Tandem structure
Transfer matrix method
Optical properties

ABSTRACT

The use of a black silicon (b-Si) interlayer is a promising solution for improving the optical properties of crystalline Si/perovskite solar cells. Optical numerical simulation of the crystalline Si/b-Si/perovskite structures can efficiently optimize their parameters at the initial tandem solar cell design stage. In this work, the optical properties of these structures were modeled using the transfer matrix method, where an array of cone-like nanoneedles of the b-Si interlayer is approximated as a homogeneous optical medium, for which the effective complex refractive index is the weighted average of those for Si and perovskite. Analytical equations are obtained for tandem structures' reflection, transmission, and absorption. The simulated reflectance spectra of the structures were compared with those of structures without the b-Si layer, as well as with experimental data. Numerical calculations and experiments confirm that nanotexturing significantly improves the optical properties of tandem structures. In addition, the nanotextured tandem structures have a wide-angle antireflective characteristic at incidence angles less than 60°, indicating their omnidirectional light-trapping capability. The proposed simulation model satisfactorily describes the optical behavior of crystalline Si/b-Si/perovskite tandem structures and can be used to estimate their optical properties depending on various parameters. As a demonstration, a numerical analysis was performed to study the effect of the b-Si interlayer thickness on the reflection of the tandem structure.

1. Introduction

Single-junction perovskite-based solar cell is an n-i-p type optoelectrical structure, which consists of an active perovskite photoabsorber and two external charge-transport layers, namely, an electron transport layer (ETL) and a hole-transport layer (HTL) [1,2]. Transparent conductive oxides (TCO) on both sides are used as contacts. The characteristics of these solar cells have been greatly improved in recent years. In 2009, when perovskite-based solar cells were first reported, their power conversion efficiency was 3.9%. At present, its value has increased to 25.2% (the certified efficiency is 23.7%.) [3]. The bandgap (>1.55 eV) and refractive index (<3) of perovskite are optimal for solar cells in the visible and near-ultraviolet radiation ranges [4,5]. To extend the spectral response range towards infrared radiation, a perovskite-based solar cell is combined with a crystalline silicon (c-Si) absorber with a narrow bandgap (1.12 eV) [6–11]. When they form a tandem cell, their absorption spectra complement each other, greatly improving the characteristics of solar cells. Such innovative tandems use one TCO contact on the frontal surface of the perovskite-based solar cell and one contact on the back surface of the bottom c-Si solar cell. That is why two-terminal tandem solar cells in the literature received the designation 2T [9–11].

One of the main tasks of c-Si/perovskite tandem solar cells is to reduce optical reflection loss and improve light scattering. That is why antireflective micron-sized pyramidal textures are formed on the c-Si surface by chemical etching [12–17]. The possible efficiency of tandem solar cells with a pyramidal textured c-Si surface is predicted to be more than 30% [18,19]. Note that for c-Si/perovskite tandem solar cells with a microtextured surface, the recently achieved record power conversion efficiency is more than 33% [20]. However, the thickness of perovskite layers is usually 300–900 nm, so it is difficult to ensure their comfortable deposition on micron-sized textures of the c-Si substrate [21–23]. Voids and gaps in the perovskite layer lead to the formation of shunts and hence low efficiency of the solar cell. Therefore, the development of a

* Corresponding author.
E-mail addresses: agagarm@gmail.com (G. Ayvazyan), fgaspar@ysu.am (F. Gasparyan), vgasparyan@csub.edu (V. Gasparian).

https://doi.org/10.1016/j.optmat.2023.113879
Received 29 March 2023; Received in revised form 5 May 2023; Accepted 7 May 2023
Available online 16 May 2023

suitable texture that will provide optimal electronic performance and optical properties of c-Si/perovskite tandem solar cells remains a major challenge.

Nanostructured Si texture, also known as "black silicon (b-Si)", is considered an effective solution to reduce the optical reflection of Si substrates. In September 2022, we experimentally demonstrated for the first time the technological feasibility and functional advantages of using b-Si as an antireflective interlayer for c-Si/perovskite tandem structures [24]. Then (October 2022), Ying et al. presented a c-Si/perovskite tandem solar cell with a b-Si interlayer and 28.2% power conversion efficiency [25]. In our recent work (January 2023), we studied in detail the structural-phase quality (surface coverage, chemical composition, dimensionality, crystallinity, and phase purity) of perovskite layers on Si substrates with a b-Si near-surface layer [26].

Black-Si is composed of nanoscale irregularities in the form of randomly arranged needles, which leads to low reflection and effective absorption of radiation incidents on the surface [27,28]. Besides, low reflection is achieved both at normal and at oblique incidences of radiation [29,30]. The excellent antireflection behavior of b-Si is due to the gradient profile of the refractive index from an optically less dense medium to a medium with a higher density, similar to multilayer coatings [31,32]. Overall, in all aspects (technology, cost, and characteristics), the nanotexture of the b-Si surpasses the microtexture obtained by chemical etching, and at present, this material is successfully used in traditional c-Si solar cells [33–35]. However, the efficiency of single-junction solar cells based on b-Si is reduced because of the elevated carrier recombination rate due to the large surface area, which results in poor spectral characteristics, especially at short wavelengths. The reduction of such recombination is usually achieved by passivation using dielectric thin films. In the case of tandem solar cells, the need for such an additional operation is often eliminated, since ETL and HTL based on ZnO, NiO, Al_2O_3, TiO_2, SnO_2, HfO_2 are at the same time good passivation materials for b-Si [34–36].

It is an experimental fact that the optical properties of b-Si depend on the ratio of surface area to volume, which is determined by the geometrical parameters (height, periodicity, diameter) of the needles array [28,32–34]. It is logical to assume that for single-junction and tandem solar cells, the preferred values of these geometrical parameters are different. Optical simulation of c-Si/b-Si/perovskite tandem structures can efficiently optimize their parameters at the initial tandem solar cell design stage. Currently, there are several rigorous methods for accurate optical modeling of micro and nanotextured surfaces, including the finite difference time domain [36–38], the finite element method [39,40], and rigorous coupled-wave analysis [41]. However, the computational effort of these methods required limits the scope of applications. The transfer matrix method (TMM) is a potential alternative for obtaining fast simulation results of multi-layered structures [42–44]. It allows the calculation of reflectivity and transmission spectra, modeling of porosity and thickness gradients of individual layers, as well as can handle multiple wavelengths and angles of incidence irradiation. The TMM has also been used for numerical optical optimization of tandem c-Si/perovskite solar cells with planar and pyramidal textured c-Si surfaces, taking into account all constituent layers (ETL, HTL, TCO, passivation, and contact films) [44–47]. In particular, it is noted that the front-side optical reflection loss still accounts for a large portion of power loss for tandem solar cells. A preliminary estimate of the optical properties of the c-Si/b-Si/perovskite tandem structure using TMM provided the refractive indices of constituent layers are real parts is given in our previous work [48]. However, for reliable analysis, it is important to model optical properties considering the complex refractive index (real and imaginary parts).

This work is aimed at experimental investigation and modeling the optical properties of the c-Si/b-Si/perovskite structure. The main focus of the study is the front-side total reflection of tandem structures with and without the b-Si interlayer. We used a standard TMM generalized to the complex refractive index profile case for modeling. We will show the acceptability of this method for the optical analysis of tandem structures and reveal the conditions for ensuring the desired optical properties. It is shown that there is good agreement between simulation results and data of experimental measurements.

2. Experimental details

For a comparative analysis with the simulation results, experimental samples of the c-Si/perovskite (planar) and c-Si/b-Si/perovskite (nanotextured) tandem structures were fabricated and studied. The p-type 400 μ m-thick c-Si (100) wafers with a resistivity of 3.0 Ω cm were used as the initial experimental samples. The b-Si layers were produced by reactive ion etching (RIE) process using an SF_6/O_2 plasma in a home-made chamber. In this study, those values of the RIE process parameters were used that were previously chosen as the most optimal for single-junction c-Si solar cells [35]. The process pressure was 55 mTorr, gas flow rates were 75 cm^3/min and 40 cm^3/min for SF_6 and O_2, respectively. The etching time was kept constant at 10 min. As an n-type ETL a 30 nm-thick TiO_2 coating was selected, which was deposited on the b-Si surface by the ALD method [24].

Of the numerous perovskite materials for solar cells, the most representative is $CH_3NH_3PbI_{3-x}Cl_x$ metal halide perovskite, which is characterized by low production cost, good stability, and relatively low toxicity [49,50]. Therefore, in this work for realistic numerical calculations of the optical properties of tandem structures, this material was chosen. A 330 nm-thick perovskite layer was deposited from precursors of methylammonium chloride (MACl) and lead iodide (PbI_2) by the vacuum co-evaporation method. Details of the deposition process parameters are given in Ref. [26]. Fig. 1 shows schematic diagrams of the RIE and co-evaporation processes.

A JEOL JSM-6700F Scanning Electron Microscope (SEM) was used to characterize the morphology and cross-sections of the obtained samples. For a statistical assessment of the geometric parameters of b-Si, 2.5 × 2.5 μm^2 areas were analyzed. The average lateral dimensions of the irregularities were measured on top SEM images by measuring the diameter of the holes and the distances between the centers of the closest neighbor holes. The irregularities' average height (peak-to-valley depth) was measured directly in cross-sectional SEM images. The angle-dependent optical reflectance of the structures was measured using a UV-3101 PC spectrometer, integrating sphere and monochromator illuminator. The sample was rotated through an incidence angle in the range of 8°–80°.

3. Simulation model description

Fig. 2 shows the typical cross-sectional and top SEM images of the c-Si/b-Si structure before and after the deposition of the perovskite layer. It is seen from Fig. 2a that b-Si consists of conical-like spikes randomly distributed over the entire surface of the c-Si wafer. The average base diameter, periodicity, and height of irregularities for the obtained samples were 100, 150, and 640 nm, respectively. After the deposition of the perovskite layer, the geometric parameters of b-Si do not change significantly (Fig. 2b), which is due to the relatively low temperature of the co-evaporation process [51]. The perovskite layer uniformly and densely covers the b-Si surface without noticeable gaps and voids.

Based on SEM images the c-Si/b-Si/perovskite structure can be represented as a thick c-Si substrate with an array of nanocones on the surface, which are in a conformal way covered with a perovskite layer (Fig. 3a). For modeling, an array of nanocones will be considered as a homogeneous optical medium, for which the effective complex refractive index is the weighted average of those for c-Si and perovskite. Then the simulation model can be represented as a structure consisting of three layers with thicknesses t_1, t_2, and t_3, and complex refractive indices $\overline{n}_1$, $\overline{n}_2$, and $\overline{n}_3$ (Fig. 3b). The refractive index of air is $\overline{n}_0 = 1$. The surface of the structure lies in the XY plane, and a plane-polarized light is an incident on the structure in the XZ plane at an angle θ_0. The angles of

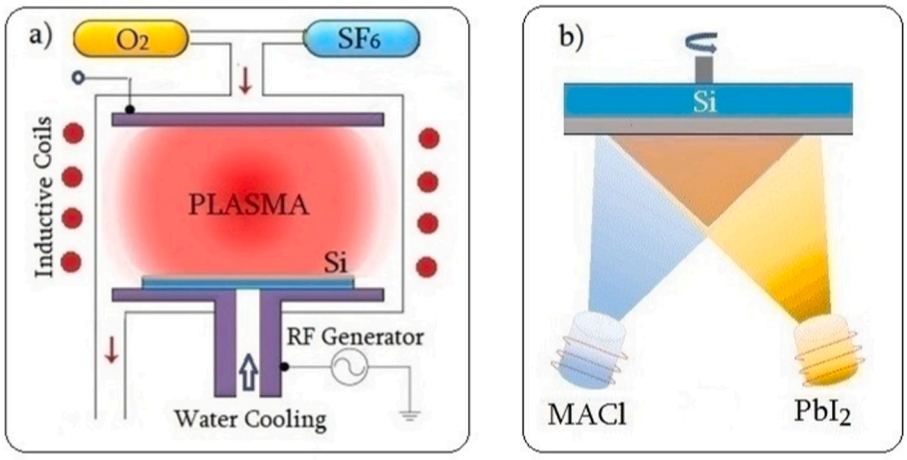

Fig. 1. Schematic diagrams of the RIE (a) and vacuum co-evaporation (b) processes.

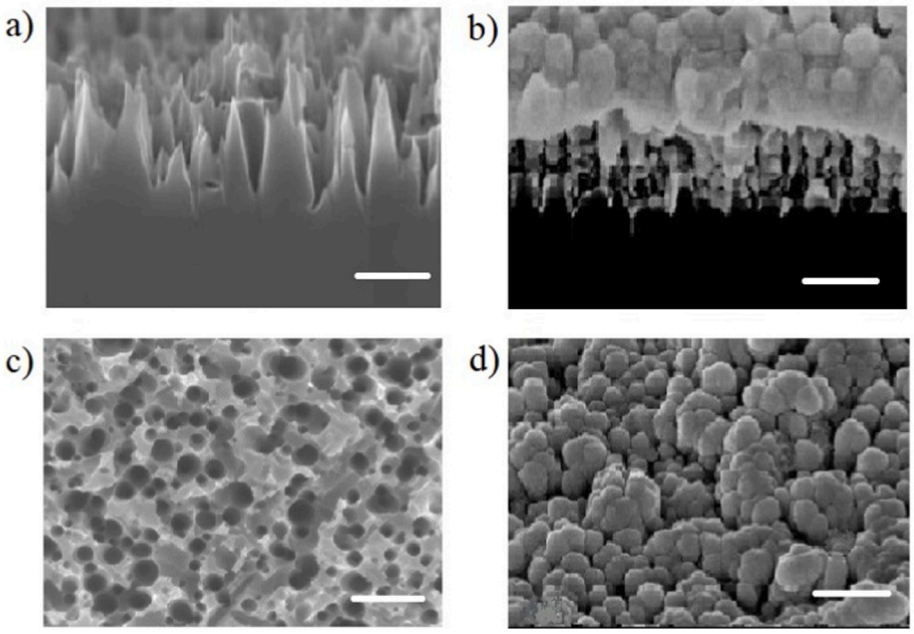

Fig. 2. Typical cross-sectional (a,b) and top (c,d) SEM images of the c-Si/b-Si structure before (a, c) and after (b, d) deposition of the perovskite layer. The scale bars represent 350 nm.

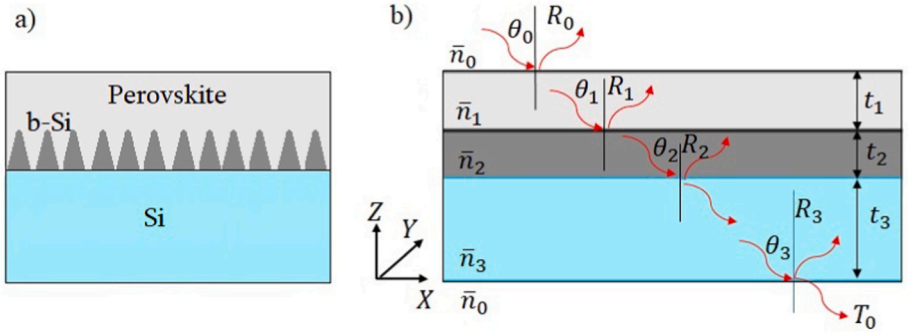

Fig. 3. Schematic illustration (a) and simulation model (b) of the structure.

incidence at the corresponding interlayer boundaries are θ_1, θ_2, and θ_3, and the reflection are R_1, R_2, and R_3. The reflection from the front surface of the structure is R_0, and the transmission from the back surface is T_0.

To determine $\bar{n}_2$, we will use the well-known Bruggeman approximation [39] which for the Si and perovskite mixture media can be

expressed according to the following Eq. (1) below:

$$(1-f)\frac{\overline{n}_3^2-\overline{n}_2^2}{\overline{n}_3^2+2\overline{n}_2^2}+f\frac{\overline{n}_1^2-\overline{n}_2^2}{\overline{n}_1^2+2\overline{n}_2^2}=0, \quad (1)$$

where f is the b-Si fill factor (i.e., the volume ratio of the c-Si/perovskite in the b-Si interlayer).

The general principle for determining the optical properties of layered media by TMM is based on the matrix formulation of the boundary conditions of the interfaces between individual layers, obtained from Maxwell's equations [42–44]. The optical properties of the considered model can be represented by a 2 × 2 matrix:

$$M_j=\begin{pmatrix} cos\ \delta_j & isin\delta_j/\gamma_j \\ i\gamma_j\ sin\ \delta_j & cos\ \delta_j \end{pmatrix}, \quad (2)$$

where $\delta_j = \frac{2\pi}{\lambda}(\overline{n}_j t_j\ cos\ \theta_j)$, $\gamma_j = \overline{n}_j\ cos\ \theta_j$, $\overline{n}_j = n_j + ik_j$, $j = 0,1,2,3$, n_j and k_j are the real and imaginary parts of the complex refractive index for the corresponding j^{th} layer, respectively, λ is the wavelength (the mathematical description of Eq. (2) transfer matrix is given in **Supporting Information).**

The reference solar spectrum AM 1.5G was used to calculate the weighted average reflectance (WAR) of the tandem structures over $\lambda = 300 - 1100\ nm$ wavelength region according to Eq. (3) [27]:

$$WAR(\lambda)=\frac{\int_{300nm}^{1100nm} R(\lambda)S(\lambda)_{AM1.5}d\lambda}{\int_{300nm}^{1100nm} S(\lambda)_{AM1.5}d\lambda}, \quad (3)$$

where $S(\lambda)_{AM1.5}$ represents the AM 1.5G solar spectrum.

4. Results and discussion

The developed simulation model makes it possible to determine the optical properties of c-Si/b-Si/perovskite tandem structures with different parameters of the constituent layers. As an example of implementation, Fig. 4 shows the simulated reflection, transmission, and absorption spectra of the c-Si/b-Si/perovskite structure. The calculations were carried out at the following fixed values of the parameters: $\theta_0 = 60^0$, $t_1 = 500\ nm$, $t_2 = 500\ nm$, $t_3 = 400\ \mu m$, $f = 0.5$. The complex refractive indices of the perovskite and c-Si were taken from the Palik material library of the software. Simulations of optical properties were performed according to Eqs. (S1)-(S3) in supporting **information** using the MatLab software package.

Fig. 5 shows experimental and simulated reflectance spectra of the planar (without b-Si layer, $f = 0$) and nanotextured (with b-Si interlayer, $f = 0.36$) tandem structures at the following values of the parameters: $\theta_0 = 8^0$, $t_1 = 330\ nm$, $t_2 = 640\ nm$, $t_3 = 400\ \mu m$. The fill factor of b-Si interlayer was calculated based on the geometrical parameters of the nanoneedles array according to the procedure presented in Ref. [37]. Contour maps of the simulated and experimental angle-resolved reflectance of these structures at $\theta_0 = 8^0 - 80^0$ in the wavelength range $\lambda = 400 - 900\ nm$ are shown in Fig. 6.

Numerical calculations and experiments confirm that nanotexturing significantly improves the optical properties of tandem structures. The reflection from the surface of planar structures is associated with a stepwise change in the refractive index during the passage of incident light from the air into the perovskite layer and then to the c-Si substrate. The b-Si layer appears as an "optically matching" medium, the refractive index of which is between perovskite and c-Si, which causes the reflection to decrease.

As seen in Fig. 5, for structures without the b-Si layer, the simulated and experimental spectra are in good agreement, especially in the visible radiation range ($\lambda = 400 - 800\ nm$), where the solar intensity is maximum. However, for nanotextured tandem structures, the experimental reflectance values over the entire wavelength range (Fig. 5) and at the considered incidence angles (Fig. 6) are noticeably lower than the calculated ones. This difference is most likely due to an approximate estimate of the complex refractive index of the b-Si interlayer. In addition, the simulation model did not take into account the fact that in real tandem structures the surface of the perovskite layer repeats the b-Si nanotexture in a smoothed form [26]. Naturally, this leads to an additional reduction in reflection. From Fig. 6 it follows that the nanotextured structures have a wide-angle antireflective characteristic, i.e.

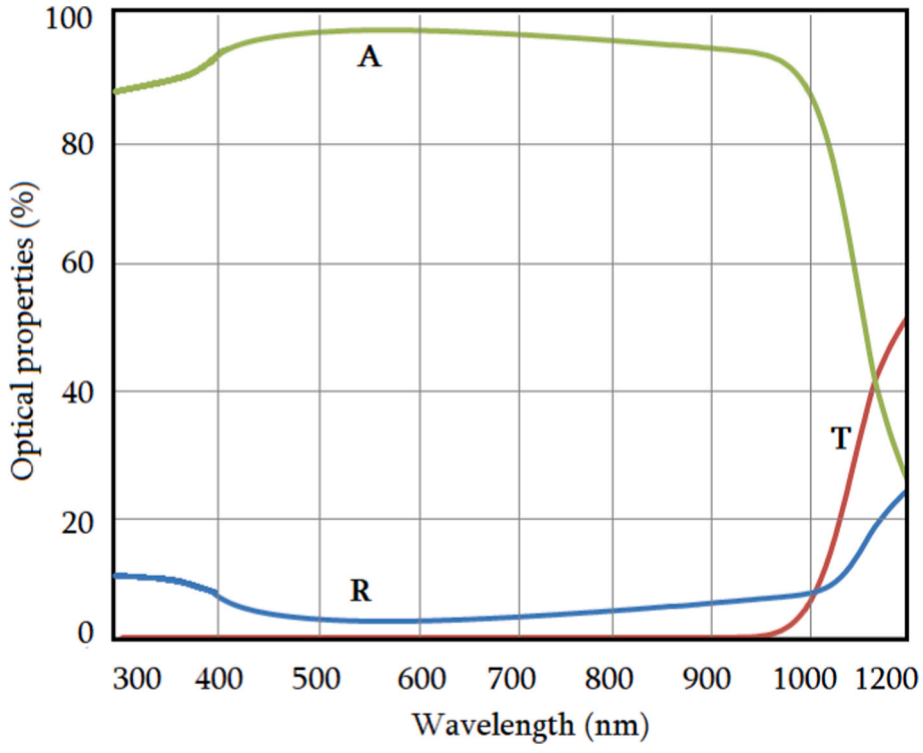

Fig. 4. Simulated reflection (R), transmission (T), and absorption (A) spectra of the c-Si/b-Si/perovskite structure.

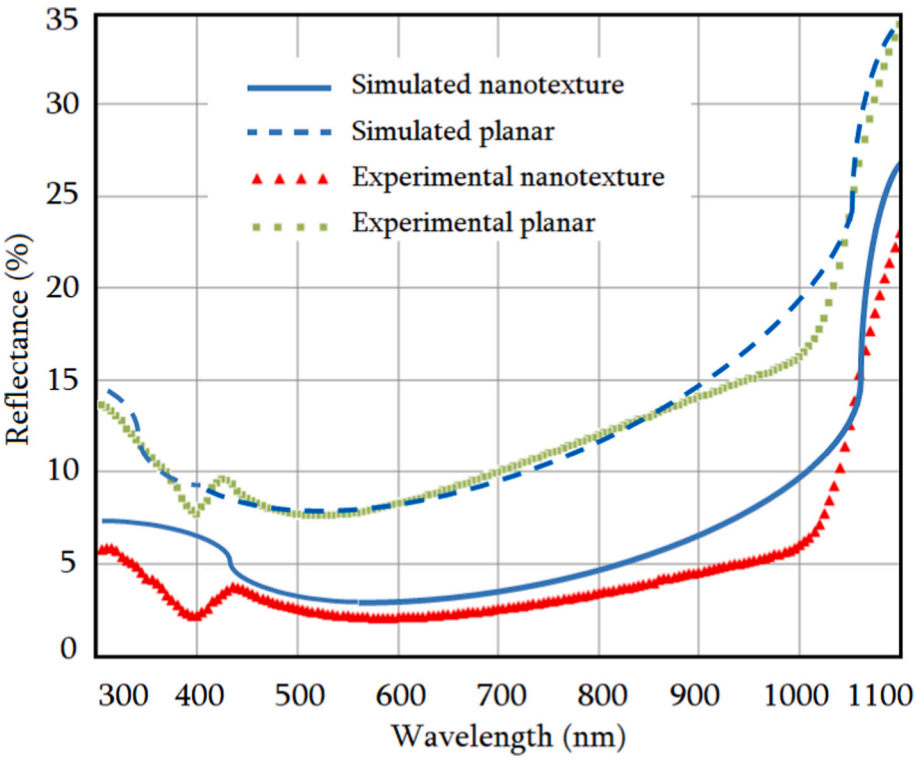

Fig. 5. Simulated reflectance spectra of the real planar and nanotextured tandem structures.

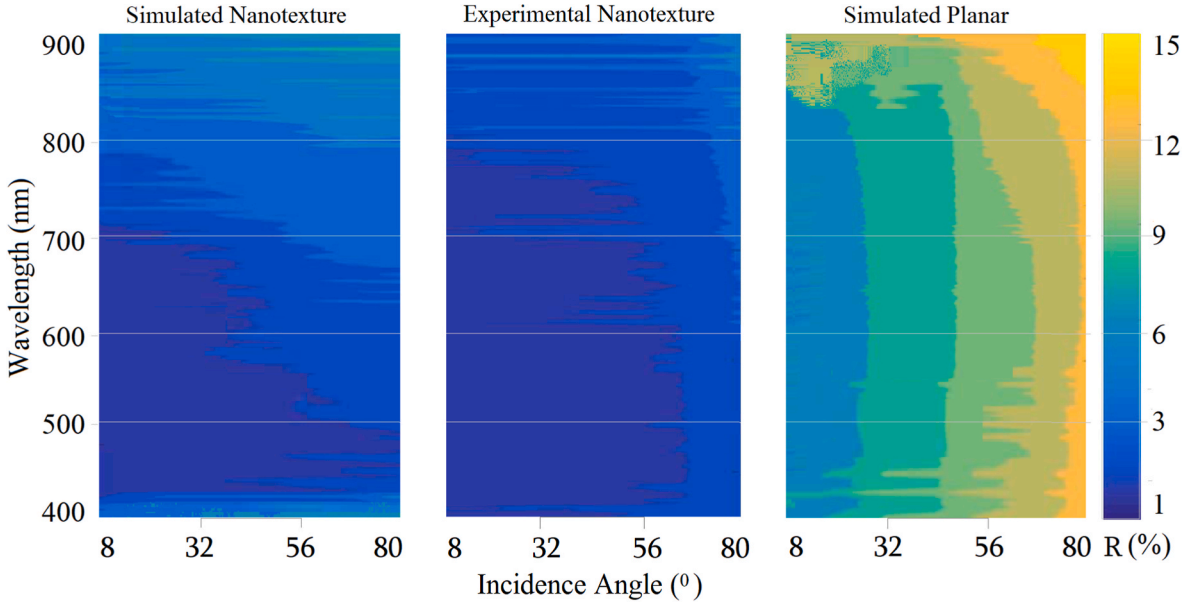

Fig. 6. Contour maps of the simulated and experimental angle-resolved reflectance of the planar and nanotextured tandem structures.

the reflection changes insignificantly at incidence angles less than 60°. This omnidirectional light-trapping ability is very important for PV stations without sun tracking for morning and evening electricity production.

Based on this study, it can be stated that the proposed simulation model satisfactorily describes the optical behavior of tandem structures and can be used to quantitatively and qualitatively evaluate their optical properties depending on various parameters. Such analysis removes the need for numerous experimental and technological reworks later. In addition, the relevance of the model extends to more general multi-layered structures with nanotextured surfaces, including the dispersion of the refractive indices of each layer [42,52]. In particular, an analysis was performed to study the effect of the b-Si interlayer thickness (height of the nanoneedles) on the reflection of the tandem structure (Fig. 7). It can be seen that as the layer thickness increases, the WAR decreases (Fig. 7a), and the minimum of the spectra shifts towards lower wavelengths (Fig. 7b). The latter feature will be the subject of future investigation. Note also that the decrease in reflection with increasing thickness almost reaches saturation at >1100 nm. Such a feature may be useful in terms of design as well as fabrication of solar cells in practice. The fact is that during thermal and chemical treatments longer needles of b-Si flatten and often break [53,54]. The choice of

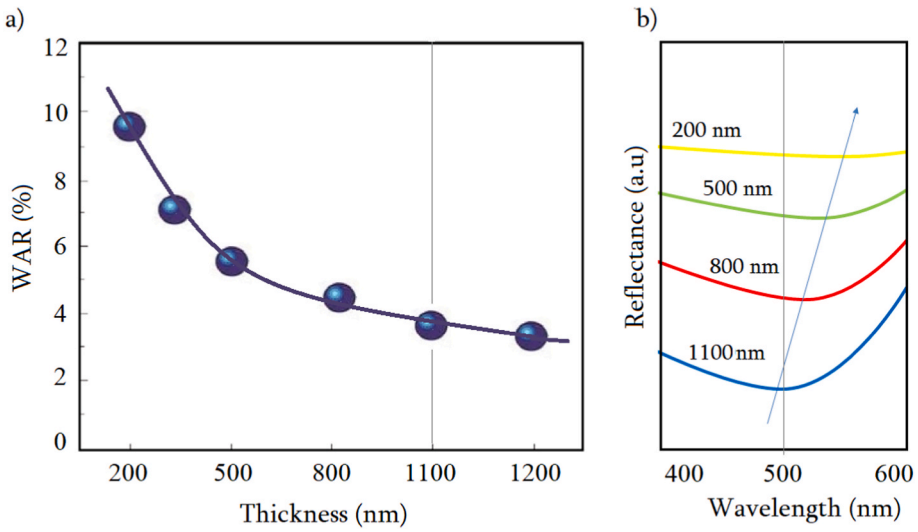

Fig. 7. WAR (a) and reflectance spectra (b) of the nanotextured tandem structures with various thicknesses of the b-Si layers.

geometrical parameters of the b-Si interlayer should be the result of compromise solutions for processes and properties optimization.

It should be noted that in the simulation model, in contrast to real c-Si/perovskite solar cells, the anti-reflective coating, transport and TCO layers, recombination, passivation and contact films were not taken into account due to their insignificant effect on the optical behavior of tandem structures [45,46].

5. Conclusions

Whilst several rigorous methods exist to accurately optical modeling of solar cell structures with micro and nanotextured surfaces, the computational effort required limits their scope. In this work, we investigated the acceptability of standard TMM for fast prediction of the optical properties of tandem c-Si/perovskite structures with a b-Si interlayer. A TMM simulation model was proposed, in which the effective complex refractive index of the b-Si interlayer is determined using the Bruggeman approximation. It is shown that b-Si significantly reduces the reflection of the tandem structures, which is maintained at incidence angles less than 60°. The numerical analysis also was performed to study the effect of the b-Si interlayer thickness on the reflection of the structures. The simulation results are in good agreement with the data of experimental measurements. Thus, the proposed simulation model satisfactorily describes the optical behavior of c-Si/b-Si/perovskite tandem structures. Its relevance extends to the more general development of solar cells with nanotextured surfaces.

CRediT authorship contribution statement

Gagik Ayvazyan: Supervision, Data curation, Investigation, Writing – original draft. **Ferdinand Gasparyan:** Conceptualization, Methodology, Investigation, Visualization. **Vladimir Gasparian:** Validation, Writing – review & editing.

Declaration of competing interest

The authors declare the following financial interests/personal relationships which may be considered as potential competing interests: Gagik Ayvazyan reports financial support was provided by Science Committee of the Ministry of Education Science Culture and Sports of the Republic of Armenia. Gagik Ayvazyan reports a relationship with National Polytechnic University of Armenia that includes: employment.

Data availability

No data was used for the research described in the article.

Acknowledgments

This work was supported by the Science Committee of the Republic of Armenia under project no. 21AG-2B011.

Appendix A. Supplementary data

Supplementary data to this article can be found online at https://doi.org/10.1016/j.optmat.2023.113879.

References

[1] F. Marangi, M. Lombardo, A. Villa, F. Scotognella, (INVITED, New strategies for solar cells beyond the visible spectral range, Opt. Mater. X 11 (2021), 100083, https://doi.org/10.1016/j.omx.2021.100083.
[2] A. Kumar, S. Singh, A. Sharma, E.M. Ahmed, Efficient and stable perovskite solar cells by interface engineering at the interface of electron transport layer/perovskite, Opt. Mater. 132 (2022), 112846, https://doi.org/10.1016/j.optmat.2022.112846.
[3] M. Green, E. Dunlop, G. Siefer, M. Yoshita, N. Kopidakis, K. Bothe, X. Hao, Solar cell efficiency tables (version 61), Prog. Photovoltaics Res. Appl. 31 (2023) 3–16, https://doi.org/10.1002/pip.3646.
[4] S.B. Khan, S. Irfan, Z. Zhuanghao, S.L. Lee, Influence of refractive index on antireflectance efficiency of thin films, Materials 12 (2019) 1483, https://doi.org/10.3390/ma12091483.
[5] A. Lamichhane, N.M. Ravindra, Energy gap-refractive index relations in perovskites, Materials 13 (2020) 1917, https://doi.org/10.3390/ma13081917.
[6] F. Fu, J. Li, T.C.-J. Yang, H. Liang, A. Faes, Q. Jeangros, C. Ballif, Y. Hou, Monolithic perovskite-silicon tandem solar cells: from the lab to fab? Adv. Math. 34 (2022), 2106540 https://doi.org/10.1002/adma.202106540.
[7] C.U. Kim, J.C. Yu, E.D. Jung, I.Y. Choi, W. Park, H. Lee, K.J. Choi, Optimization of device design for low cost and high efficiency planar monolithic perovskite/silicon tandem solar cells, Nano Energy 60 (2019) 213–221, https://doi.org/10.1016/j.nanoen.2019.03.056.
[8] A. Al-Ashouri, E. Köhnen, B. Li, A. Magomedov, H. Hempel, P. Caprioglio, S. Albrecht, Monolithic perovskite/silicon tandem solar cell with >29% efficiency by enhanced hole extraction, Science 370 (2020) 1300–1309, https://doi.org/10.1126/science.abd401.
[9] I.Y. Choi, C.U. Kim, W. Park, H. Lee, M.H. Song, K.K. Hong, K.J. Choi, Two-terminal mechanical perovskite/silicon tandem solar cells with transparent conductive adhesives, Nano Energy 65 (2019), 104044, https://doi.org/10.1016/j.nanoen.2019.104044.
[10] Y. Hu, L. Song, Y. Chen, W. Huan, Two-Terminal perovskites tandem solar cells: recent advances and perspectives, Solar RRL 3 (2019), 1900080, https://doi.org/10.1002/solr.201900080, 2019.
[11] M. Haider, J.-L. Yang, Efficient and stable perovskite–silicon two-terminal tandem solar cells, Rare Met. 39 (2020) 745–747, https://doi.org/10.1007/s12598-020-01430-4.

[12] K. Hamada, K. Yonezawa, K. Yamamoto, T. Taima, S. Hayase, N. Ooyagi, Y. Yamamoto, K. Ohdaira, Vacuum deposition of $CsPbI_3$ layers on textured Si for perovskite/Si tandem solar cells, Jap. J. Appl. Phys. 58 (2019) SBBF06, https://doi.org/10.7567/1347-4065/aafb56.

[13] L. Gil-Escrig, M. Roß, J. Sutter, A. Al-Ashouri, C. Becker, S. Albrecht, Fully vacuum-processed perovskite solar cells on pyramidal microtextures, Solar RRL 5 (2020), 2000553, https://doi.org/10.1002/solr.202000553.

[14] M. Jošt, E. Köhnen, A.B. Morales-Vilches, B. Lipovšek, K. Jäger, B. Macco, A. Al-Ashouri, J. Krč, L. Korte, B. Rech, R. Schlatmann, M. Topič, B. Stannowski, S. Albrecht, Textured interfaces in monolithic perovskite/silicon tandem solar cells: advanced light management for improved efficiency and energy yield, Energy Environ. Sci. 11 (2018) 3511–3523, https://doi.org/10.1039/C8EE02469C.

[15] R. Wang, T. Huang, J. Xue, J. Tong, K. Zhu, Y. Yang, Prospects for metal halide perovskite-based tandem solar cells, Nat. Photonics 15 (2021) 411–425, https://doi.org/10.1038/s41566-021-00809-8.

[16] B. Chen, Z.S.J. Yu, S. Manzoor, S. Wang, W. Weigand, Z.H. Yu, G. Yang, Z.Y. Ni, X. Z. Dai, Z.C. Holman, J.S. Huang, Blade-Coated perovskites on textured silicon for 26%-efficient monolithic perovskite/silicon tandem solar cells, Joule 4 (2020) 850–864, https://doi.org/10.1016/j.joule.2020.01.008.

[17] E.M. Tennyson, K. Frohna, W.K. Drake, F. Sahli, T. Yang, T. Fu, S.D. Stranks, Multimodal microscale imaging of textured perovskite–silicon tandem solar cells, ACS Energy Lett. 6 (2021) 2293–2304, https://doi.org/10.1021/acsenergylett.1c00568.

[18] B.W. Schneider, N.N. Lal, S. Baker-Finc, T.P. White, Pyramidal surface textures for light trapping and antireflection in perovskite-on-silicon tandem solar cells, Opt Express 22 (2014) A1422–A1430, https://doi.org/10.1364/OE.22.0A1422.

[19] M.I. Hossain, W. Qarony, V. Jovanov, Y.H. Tsang, D. Knipp, Nanophotonic design of perovskite/silicon tandem solar cells, J. Mater. Chem.A 6 (2018) 3625–3633, https://doi.org/10.1039/C8TA00628H.

[20] KAUST claims 33.2% efficiency for perovskite/silicon tandem solar cell. https://www.pv-magazine.com/2023/04/13/kaust-claims-33-2-efficiency-for-perovskite-silicon-tandem-solar-cell/, 2023, 05 May 2023.

[21] B. Salhi, Y.S. Wudil, M.K. Hossain, A. Al-Ahmed, F.A. Al-Sulaiman, Review of recent developments and persistent challenges in stability of perovskite solar cells, Renew. Sustain. Energy Rev. 90 (2018) 210–222, https://doi.org/10.1016/j.rser.2018.03.058.

[22] Q. Guesnay, F. Sahli, C. Ballif, Q. Jeangros, Vapor deposition of metal halide perovskite thin films: process control strategies to shape layer properties, Apl. Mater. 9 (2021), 100703, https://doi.org/10.1063/5.0060642.

[23] L. Cojocaru, K. Wienands, T.W. Kim, S. Uchida, A.J. Bett, S. Rafizadeh, J. C. Goldschmidt, S.W. Glunz, Detailed investigation of evaporated perovskite absorbers with high crystal quality on different substrates, ACS Appl. Mater. Interfaces 10 (2018) 26293–26302, https://doi.org/10.1021/acsami.8b07999.

[24] G.Y. Ayvazyan, D.L. Kovalenko, M.S. Lebedev, L.A. Matevosyan, A.V. Semchenko, Investigation of the structural and optical properties of silicon-perovskite structures with a black silicon layer, J. Contemp. Phys. 57 (2022) 274, https://doi.org/10.1134/S1068337222030069.

[25] Z. Ying, Z. Yang, J. Zheng, H. Wei, L. Chen, C. Xiao, J. Sun, C. Shou, G. Qin, J. Sheng, Y. Zeng, B. Yan, X. Yang, J. Ye, Monolithic perovskite/black-silicon tandems based on tunnel oxide passivated contacts, Joule 6 (2022) 2644–2661, https://doi.org/10.1016/j.joule.2022.09.006.

[26] A. Vaseashta, G. Ayvazyan, S. Khudaverdyan, L. Matevosyan, Structural and optical properties of vacuum-evaporated mixed-halide perovskite layers on nanotextured black silicon, Phys. Status Solidi RRL 17 (2023), 2200482, https://doi.org/10.1002/pssr.202200482.

[27] S. Uddin, R. Hashim, M.Z. Pakhuruddin, Broadband light absorption enhancement in nanoporous black silicon synthesized by aluminium-catalyzed chemical etching, Opt. Mater. 134 (2022), 113111, https://doi.org/10.1016/j.optmat.2022.113111.

[28] F. Atteia, J. Le, L. Denaix, D. Duché, G. Berginc, J.J. Simon, L. Escoubas, Morphologies and optical properties of black silicon by room temperature reactive ion etching, Mater. Res. Bull. 131 (2020), 110973, https://doi.org/10.1016/j.materresbull.2020.110973.

[29] R.S. Davidsen, J. Ormstrup, M.L. Ommen, P.E. Larsen, M.S. Schmidt, A. Boisen, Q. Nordseth, O. Hansen, Angle resolved characterization of nanostructured and conventionally textured silicon solar cells, Solar Energy Mat, Sol. Cell. 140 (2015) 134–140, https://doi.org/10.1016/j.solmat.2015.04.001.

[30] W.Q. Xie, J.I. Oh, W.Z. Shen, Realization of effective light trapping and omnidirectional antireflection in smooth surface silicon nanowire arrays, Nanotechnology 22 (2011), 065704, https://doi.org/10.1088/0957-4484/22/6/065704.

[31] S. Ma, S. Liu, Q. Xu, J. Xu, J. Lu, Y. Liu, Z. Zhong, A theoretical study on the optical properties of black silicon, AIP Adv. 8 (2018), 035010, https://doi.org/10.1063/1.5018642.

[32] S. Wang, T. Xie, R. Liang, Y. Zhang, F.-J. Ma, D. Payne, G. Scardera, B. Hoex, An artificial-antelligence-assisted investigation on the potential of black silicon nanotextures for silicon solar cells, ACS Appl. Nano Mater. 5 (2022) 11636–11647, https://doi.org/10.1021/acsanm.2c02619.

[33] X. Liu, P. Coxon, M. Peters, B. Hoex, J. Cole, D. Frayc, Black silicon: fabrication methods, properties and solar energy applications, Energy Environ. Sci. 7 (2014) 3223–3263, https://doi.org/10.1039/C4EE01152J.

[34] M. Otto, M. Algasinger, H. Branz, B. Gesemann, T. Gimpel, K. Füchsel, T. Käsebier, S. Kontermann, S. Koynov, X. Li, V. Naumann, J. Oh, A. Sprafke, J. Ziegler, M. Zilk, R. Wehrspoh, Black silicon photovoltaics, Adv. Opt. Mater. 3 (2015) 147–164, https://doi.org/10.1002/adom.201400395.

[35] G.Y. Ayvazyan, R.N. Barseghyan, S.A. Minasyan, Optimization of surface reflectance for silicon solar cells, in: E3S Web Conf., vol. 69, 2018, 01008, https://doi.org/10.1051/e3sconf/20186901008.

[36] M.V. Katkov, G.Y. Ayvazyan, V.R. Shayapov, M.S. Lebedev, Modeling of the optical properties of black silicon passivated by thin films of metal oxides, J. Contemp. Phys. 55 (2020) 16–22, https://doi.org/10.3103/S106833722001003X.

[37] T. Rahman, S.A. Boden, Optical modeling of black silicon for solar cells using effective index techniques, IEEE J. Photovoltaics 7 (2017) 1556–1562, https://doi.org/10.1109/JPHOTOV.2017.2748900.

[38] D. Shi, Y. Zeng, W. Shen, Perovskite/c-Si tandem solar cell with inverted nanopyramids: realizing high efficiency by controllable light trapping, Sci. Rep. 5 (2015), 16504, https://doi.org/10.1038/srep16504.

[39] S. Zandi, M. Razaghi, Finite element simulation of perovskite solar cell: a study on efficiency improvement based on structural and material modification, Sol. Energy 179 (2019) 298–306, https://doi.org/10.1016/j.solener.2018.12.032.

[40] K. Jäger, J. Sutter, M. Hammerschmidt, P.I. Schneider, C. Becker, Prospects of light management in perovskite/silicon tandem solar cells, Nanophotonics 10 (2021) 1991–2000, https://doi.org/10.1515/nanoph-2020-0674.

[41] A.J. Bett, J. Eisenlohr, O. Höhn, P. Repo, H. Savin, B. Bläsi, J.C. Goldschmidt, Wave optical simulation of the light trapping properties of black silicon surface textures, Opt Express 24 (2016) A434–A445, https://doi.org/10.1364/OE.24.00A434.

[42] M. Bellingeri, A. Chiasera, I. Kriegel, F. Scotognella, Optical properties of periodic, quasi-periodic, and disordered one-dimensional photonic structures, Opt. Mater. 72 (2017) 403–421, https://doi.org/10.1016/j.optmat.2017.06.033.

[43] A.A. Elsayed, T.M. Sabry, F. Marty, T. Bourouina, K. Khalil, Optical modeling of black silicon using an effective medium/multi-layer approach, Opt Express 26 (2018) 13443–13460, https://doi.org/10.1364/OE.26.013443.

[44] C. Gao, D. Du, W. Shen, Monolithic perovskite/c-Si tandem solar cell: progress on numerical simulation, Carbon Neutrality 1 (2022) 9, https://doi.org/10.1007/s43979-022-00003-x.

[45] R. Santbergen, R. Mishima, T. Meguro, M. Hino, H. Uzu, J. Blanker, K. Yamamoto, M. Zeman, Minimizing optical losses in monolithic perovskite/c-Si tandem solar cells with a flat top cell, Opt Express 24 (2016) A1288–A1299, https://doi.org/10.1364/OE.24.0A1288.

[46] K. Jäger, L. Korte, B. Rech, S. Albrecht, Numerical optical optimization of monolithic planar perovskite-silicon tandem solar cells with regular and inverted device architectures, Opt Express 25 (2017) A473–A482, https://doi.org/10.1364/OE.25.00A473.

[47] F.E. Cherif, H. Sammouda, Strategies for high performance perovskite/c-Si tandem solar cells: effects of bandgap engineering, solar concentration and device temperature, Opt. Mater. 106 (2020), 109935.

[48] F.V. Gasparyan, G.Y. Ayvazyan, Reflection and transmission of radiation of the structure crystalline silicon–black silicon–perovskite, J. Contemp. Phys. 57 (2022) 160, https://doi.org/10.1016/j.optmat.2020.109935.

[49] Z. Gevorkian, V. Gasparian, Y. Lozovik, Large diffusion lengths of excitons in perovskite and TiO_2 heterojunction, Appl. Phys. Lett. 108 (2016), 051109, https://doi.org/10.1063/1.4941242.

[50] B.A. Al-Asbahi, M.H. Saif, S.M.H. Qaid, M. Hezam, I. Bedja, H.M. Ghaithan, A. S. Aldwayyan, Effect of deposition method on the structural and optical properties of $CH_3NH_3PbI_3$ perovskite thin films, Opt. Mater. 103 (2020), 109836, https://doi.org/10.1016/j.optmat.2020.109836.

[51] G. Ayvazyan, A. Vaseashta, F. Gasparyan, S. Khudaverdyan, Effect of thermal annealing on the structural and optical properties of black silicon, J. Mater. Sci. Mater. Electron. 33 (2022) 17001–17010, https://doi.org/10.1007/s10854-022-08578-y.

[52] M. Sygletou, F. Marangi, S. Varas, A. Chiasera, M. Canepa, F. Scotognella, F. Bisio, Effective medium optical modelling of indium tin oxide nanocrystal films, Phys. Chem. Chem. Phys. 24 (2022) 5317–5322, https://doi.org/10.1039/D1CP05897E.

[53] G. Ayvazyan, L. Hakhoyan, K. Ayvazyan, A. Aghabekyan, External gettering of metallic impurities by black silicon layer, Phys. Status Solidi A 220 (2023), 2200793, https://doi.org/10.1002/pssa.202200793.

[54] T.P. Pasanen, H.S. Laine, V. Vahanissi, K. Salo, S. Husein, H. Savin, Impact of standard cleaning on electrical and optical properties of phosphorus-doped black silicon, IEEE J. Photovoltaics 8 (2018) 697–702, https://doi.org/10.1109/JPHOTOV.2018.2806298.